Phys Chem Minerals (2015) 42:203–212
DOI 10.1007/s00269-014-0711-z

ORIGINAL PAPER

Elasticity of single-crystal quartz to 10 GPa

Jue Wang · Zhu Mao · Fuming Jiang · Thomas S. Duffy

Received: 5 June 2014 / Accepted: 15 September 2014 / Published online: 26 September 2014

Abstract The second-order elastic constants of quartz were determined by Brillouin spectroscopy to 10 GPa in a diamond anvil cell. All elastic constants exhibit smooth pressure trends. A decrease in the magnitudes of C_{14} and C_{66} with pressure is observed, while C_{44} shows a weak pressure dependence. Our measured elastic constants are more consistent with previous density functional theory calculations than with earlier experimental results. Aggregate elastic moduli were calculated and fit to a finite-strain equation of state, yielding values for the pressure derivatives of the adiabatic bulk modulus, K_{0S}', and shear modulus, G_0', of α-quartz of 6.2(2) and 0.9(1), respectively. The equation of state obtained from our data is consistent with static X-ray diffraction data. A finite-strain extrapolation of our data predicts a violation of a Born stability criterion, indicating a mechanical instability in the structure, at ~26 GPa which is broadly consistent with the pressure range at which a phase transition and pressure-induced amorphization in quartz are observed.

Keywords Elasticity · Quartz · High pressure

Introduction

Quartz is a geologically abundant and technically important mineral (Hemley 1987; Heaney et al. 1994; Ballato 2008). It is one of the most common minerals in the Earth's crust, and SiO_2 is the major oxide component of Earth's interior. Quartz is widely used in technical applications as an oscillator and piezoelectric material (Ballato 2008). Quartz and its many polymorphs exhibit a rich and complex response to compression (Hemley et al. 1994). The elastic properties of quartz at high pressure are important for understanding its sound velocities, mechanical behavior, and phase transition mechanism.

α-Quartz is the stable polymorph of SiO_2 at ambient conditions and has trigonal symmetry (space group $P3_121$ or $P3_221$). The structure of quartz can be described as a framework of SiO_4 tetrahedra forming a pair of spiral chains running along the *c*-axis. At ambient conditions, the bulk modulus of quartz is ~37 GPa, so the structure is more compressible than many other silicates. It is also anisotropic as the *a* axis is ~50 % more compressible than *c*-axis (Hazen et al. 1989; Angel et al. 1997). The high-pressure behavior of quartz has been studied previously in a number of single-crystal X-ray diffraction studies (Levien et al. 1980; Hazen et al. 1989; Glinnemann et al. 1992; Angel et al. 1997). Compression is primarily taken up by changes in Si–O–Si angles and inter-tetrahedral O–O distances. The SiO_4 tetrahedra are largely incompressible, but distortion of the tetrahedra increases with pressure. By 15 GPa, the oxygen ions approach a close-packed configuration, and the *c*-axis channels are nearly closed (Hazen et al. 1989).

Under high pressure–temperature conditions, quartz transforms to coesite at ~2.5 GPa and 900 K (Mirwald and Massonne 1980). When compressed at room temperature, quartz persists metastably to above 20 GPa. X-ray diffraction experiments originally reported that α-quartz undergoes pressure-driven amorphization at 15–35 GPa and 300 K (Hemley et al. 1988; Kingma et al. 1993b; Williams et al. 1993). Later an angle-dispersive X-ray diffraction

J. Wang (✉) · Z. Mao · F. Jiang · T. S. Duffy
Department of Geosciences, Princeton University, Princeton, NJ 08544, USA
e-mail: juewang@princeton.edu

Present Address:
Z. Mao
University of Science and Technology of China, Hefei 230026, Anhui, China

experiment found that α-quartz transformed to a new phase (quartz II) with an unknown structure at 21 GPa and subsequently became amorphous above 30 GPa (Kingma et al. 1993a). At 40 GPa, a new monoclinic structure built up of zigzag chains of SiO_6 octahedra was synthesized (Haines et al. 2001). The response of quartz to compression appears to be sensitive to experimental conditions (e.g., amount of shear stress, rate of compression), and the resultant phases are difficult to study as they may be poorly crystalline and/or heterogeneous. Theoretical calculations indicate that quartz exhibits elastic softening and phonon instabilities which may be driving forces for amorphization and phase transitions (Binggeli and Chelikowsky 1992; Binggeli et al. 1994).

While numerous studies of the elastic constants of quartz have been performed at ambient pressure (McSkimin et al. 1965; Every and McCurdy 1992; Holm and Ahuja 1999; Heyliger et al. 2003; Lakshtanov et al. 2006; Ohno et al. 2006; Ogi et al. 2006; Tarumi et al. 2007), the high-pressure elasticity of quartz is poorly constrained (McSkimin et al. 1965; Wang et al. 1992; Gregoryanz et al. 2000; Choudhury and Chaplot 2006; Kimizuka et al. 2007; Calderon et al. 2007). High-pressure experimental studies by Brillouin scattering (Gregoryanz et al. 2000) and ultrasonic techniques (McSkimin et al. 1965; Wang et al. 1992; Calderon et al. 2007) show large inconsistencies with each other and with the results of theoretical studies using density functional theory (DFT) (Choudhury and Chaplot 2006; Kimizuka et al. 2007). Here, we report the single-crystal elasticity of α-quartz up to 10 GPa under hydrostatic compression by Brillouin spectroscopy to resolve discrepancies in previous studies and to better understand the mechanical response of quartz to compression.

Experimental details

Experiments were performed using optical-grade single crystals of synthetic untwined quartz (MTI Corporation). Two orientations were used: x-cut (110) and z-cut (001). The samples were characterized by Raman spectroscopy and X-ray diffraction to confirm the quality of the crystals. The unit cell parameters of the sample at ambient conditions are as follows: $a = 4.914$ Å and $c = 5.405$ Å with density 2.648 g/cm^3.

Crystal platelets of ~100-μm diameter were double-side-polished to ~35-μm thickness. The platelets were loaded into wide-angle diamond anvil cells (DAC) with 500-μm diameter culets. A 16:3:1 methanol–ethanol–water (MEW) mixture was used to provide a hydrostatic medium for experiments up to 10 GPa (Angel et al. 2007). Four rubies were distributed around the sample as pressure markers using the ruby fluorescence technique (Mao et al. 1986). At each pressure step, the diamond cells were adjusted until pressures were the same for each platelet to within about 0.1 GPa. The ruby peaks remained sharp at all pressures with peak widths only slightly broadened relative to ambient values. Pressures from four different ruby positions around the sample are in agreement to within 0.3 % or better up to highest pressure measured. In order to allow for pressure stabilization, at least 6 h elapsed after each pressure change before beginning the Brillouin measurements.

For each platelet, Brillouin spectra were collected at room temperature in four pressure steps up to 10.2 GPa. All spectra were measured in a symmetric forward scattering geometry with an angle of 35° between the incident and scattered beam. A 150-mW solid-state laser (532.15 nm wavelength) was used to excite Brillouin spectra. The scattered radiation was collected using a six-pass tandem Fabry–Perot interferometer. Spectra were typically collected at 10° intervals over a 180° range at each pressure step. The average exposure time for each measurement was 5–10 min. In the forward symmetric scattering geometry, the acoustic velocity, V, can be determined independent of the refractive index of the sample at high pressure (Whitfield et al. 1976). The measured Brillouin frequency shift, $\Delta\nu$, is related to acoustic velocity V through the relation: $V = \Delta\nu\lambda_0/2\sin\theta$, where λ_0 is incident laser wavelength and θ is the scattering angle. Figure 1a shows a representative Brillouin spectrum collected at 4.4 GPa. There are peaks corresponding to a quasi-longitudinal mode (V_P), the pressure medium (MEW) and a quasi-transverse mode (V_{S1}). We estimate there is ±0.5–1 % uncertainty in the measured velocities based on measurements of calibrated standards. Further details regarding the Brillouin scattering system can be found elsewhere (Speziale and Duffy 2002).

Results and discussion

At all pressures, we detected two modes (one quasi-longitudinal and one quasi-shear) in the (110) platelet (x-cut) and either two or three modes (two quasi-shear and one quasi-longitudinal) in the (001) platelet (z-cut). The absence of one of the two shear modes in some directions may result from weak elasto-optic coupling. Overlap of shear modes with peaks of the pressure medium also occurred in certain directions for pressures below 7 GPa. In addition, the refractive indices of quartz and the pressure medium become nearly identical around 8 GPa restricting measurements in this range due to inability to visualize the sample.

Quartz has six independent elastic constants: C_{11}, C_{33}, C_{12}, C_{13}, C_{14} and C_{44}. At each pressure, the elastic tensor was determined through the nonlinear least-squares inversion of the Christoffel equation (Every 1980). The inversion process was iterative. Initially, the C_{ij}s of quartz were

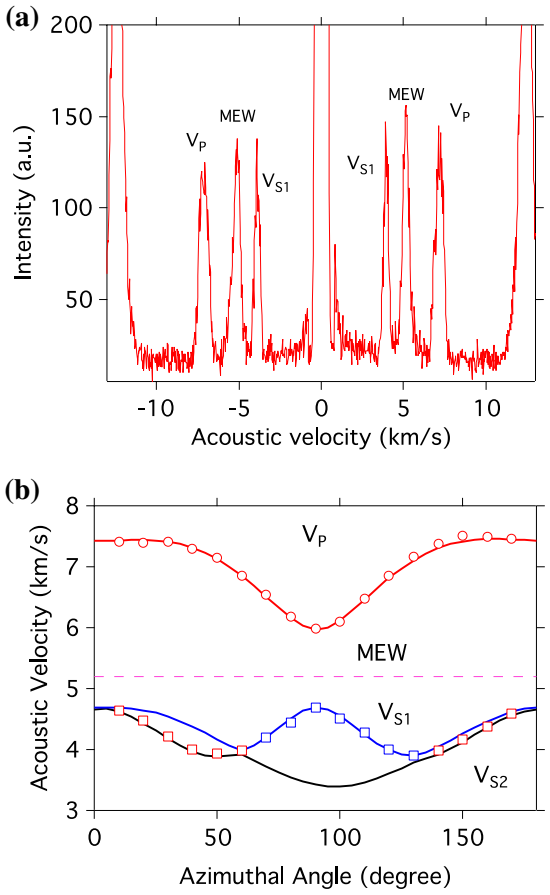

Fig. 1 **a** Brillouin spectrum for x-cut quartz at 4.4 GPa. V_{S1}, quasi-transverse acoustic mode; V_P, quasi-longitudinal acoustic mode; *MEW* methanol–ethanol–water mixture. The measured Brillouin frequency shift has been converted to acoustic velocity. **b** Measured velocity data for quartz at 4.4 GPa as a function of crystal direction. *Symbols* experimental data; *solid line* best-fitting velocity curves. Azimuthal angles are measured relative to an arbitrary initial value. V_P: Quasi-longitudinal acoustic mode; V_{S1} and V_{S2}: Quasi-transverse or transverse acoustic modes

estimated from linear extrapolation of lower pressure values, and the orientations of the planes were fixed during initial inversion. The resulting C_{ij} values were then further refined by allowing the orientation of the x-cut plane to vary slightly (~1°–2°) while either holding the C_{ij}s fixed or allowing them to vary simultaneously as well. The lack of anisotropy normal to [001] precluded including the orientation of the z-cut plane in the inversion.

An iterative procedure was also adopted to refine the initial density model, and the individual and aggregate moduli. The elastic moduli of quartz at ambient conditions have been measured in many studies and are well constrained. We used the average of twelve previous measurements reported in the Landolt–Börnstein Tables (Every and McCurdy 1992) which are also consistent with more recent measurements (Heyliger et al. 2003; Ogi et al. 2006; Ohno et al. 2006; Lakshtanov et al. 2006; Tarumi et al. 2007). Voigt and Reuss bounds on the aggregate bulk and shear moduli and Voigt-Reuss-Hill averages (Hill 1963) were computed from the individual moduli at ambient and high pressure. We then fit a third-order finite-strain equation (Birch 1978) to the Reuss bound of the bulk modulus in order to obtain the ambient-pressure adiabatic (Reuss) bulk modulus, K_{0S}, and its pressure derivative, $K'_{0S} = (\partial K_{0S}/\partial P)_T$. These values were then corrected to corresponding isothermal values K_{0T} and K'_{0T} using known thermodynamic parameters for quartz (Table 1). The expressions used for this calculation are given elsewhere (Speziale and Duffy 2002; Zouboulis et al. 2014). The resulting Reuss bound on the isothermal bulk modulus together with its pressure derivative was used to calculate densities at high pressure using the Birch-Murnaghan equation:

$$P = \frac{3}{2}K_{0T}\left[\left(\frac{V_0}{V}\right)^{\frac{7}{3}} - \left(\frac{V_0}{V}\right)^{\frac{5}{3}}\right]\left\{1 + \frac{3}{4}(K'_{0T} - 4)\left[\left(\frac{V_0}{V}\right)^{\frac{2}{3}} - 1\right]\right\} \quad (1.1)$$

These new density values were then used to compute a refined set of C_{ij}s, and the procedure was iterated until convergence. The difference between initial and final densities was less than 0.3 % at all pressures. The final sets of elastic constants and density values are listed in Table 2. Figure 1b shows the measured velocities at a representative pressure compared with calculated values from the best-fitting elastic constants. The quality of the fit is good as demonstrated by the low root-mean-square (RMS) difference between the observed and calculated velocities (Table 2).

α-Quartz is a piezoelectric material. For such a material, an applied stress creates an electric field as well as a strain field in the crystal. Incorporation of the piezoelectric effect

Table 1 Thermoelastic parameters of quartz

Parameter	Value	Reference
Thermal expansivity, α	4.31 (4) × 10^{-5} K^{-1}	Ackerman and Sorrell (1974)
Specific heat, C_P	746.3 (1) J kg^{-1} K^{-1}	Hemingway (1987)
Grüneisen parameter, γ	0.84 (7)	Calculated
$(\partial K_T/\partial T)_{P0}$	−0.014 GPa K^{-1}	Ohno (1995)
K_{T0}	37.12 (9) GPa	Angel et al. (1997)
K_{T0}'	5.99 (4)	Angel et al. (1997)
K_{T0}	37.4 (6) GPa	This study
K_{T0}'	6.2 (2)	This study

Grüneisen parameter is calculated using $\gamma = \alpha K_{S0}/(\rho_0 C_P)$, where ρ_0 is density at ambient conditions

K_{T0}: isothermal bulk modulus at ambient pressure

K_{T0}': pressure derivative of the isothermal bulk modulus at ambient pressure

Table 2 Elastic constants of α-quartz

P (GPa)	ρ (g/cm^3)	C_{11} (GPa)	C_{33} (GPa)	C_{12} (GPa)	C_{13} (GPa)	C_{14} (GPa)	C_{44} (GPa)	K_{0S}(GPa)	G_0 (GPa)	RMS (km/s)
10^{-4}	2.648	86.6 (3)	106.4 (12)	6.74 (9)	12.4 (16)	17.8 (3)	58.0 (7)	37.8	44.4	
1.5	2.742	90.3 (8)	122.3 (15)	15.4 (100)	23.7 (21)	10.7 (10)	62.4 (10)	48.3	46.8	0.087
4.4	2.897	103.4 (3)	160.1 (10)	35.6 (6)	38.9 (10)	3.8 (7)	63.6 (4)	64.2	47.4	0.040
6.9	3.004	115.7 (20)	190.6 (19)	47.1 (20)	50.6 (14)	0.3 (1)	65.4 (5)	77.0	49.4	0.058
10.2	3.120	127.5 (5)	217.0 (10)	61.3 (7)	62.0 (12)	−1.9 (8)	65.9 (3)	89.6	49.2	0.054

For C_{ij}s, numbers in parentheses represent one standard deviation uncertainties in the last digit(s)

Ambient values are an average of 12 previous studies compiled in Every and McCurdy (1992)

K_{0S} and G_0 refer to Voigt-Reuss-Hill averages of the individual elastic moduli

ANSI/IEEE Standard 176-1988 is used to assign the sign of C_{14}

RMS root-mean-square deviation between measured and best-fit velocities

requires consideration of piezoelectric stress–strain equations, which depend on the piezoelectric stress constants and the dielectric tensor. Quartz has two independent piezoelectric and two independent dielectric constants. Studies at ambient pressure have shown that elastic constants differ by at most 0.5 % due to incorporation of piezoelectricity in the Christoffel equation (Ohno 1990). As a result, we have ignored the effects of piezoelectricity in this study as was also done in previous high-pressure elasticity studies (Gregoryanz et al. 2000).

The elastic constants of quartz at high pressure are shown in Fig. 2. C_{11}, C_{33}, C_{12}, and C_{13} all increase strongly with pressure, whereas C_{44} shows only a weak increase. C_{14} and C_{66} [defined as $1/2(C_{11} - C_{12})$] decrease with compression. The (one sigma) uncertainties for individual C_{ij}s at each pressure are given in Table 2. Our measurements provide the tightest constraints on the longitudinal moduli, C_{11} and C_{33}, and the shear modulus, C_{44}, and their uncertainties are within 2 %. The uncertainties are larger and more variable for the off-diagonal moduli. At 1.5 GPa, the uncertainties in the C_{ij}s are larger because velocities in some directions could not be measured due to overlap between the slow shear wave and pressure medium peaks for the z-cut platelet. This results in covariance among the fitted elastic constants, and as a result, C_{12} is poorly constrained at this pressure.

The individual C_{ij}s were fit to third-order finite-strain equations (red curves in Fig. 2) using (Birch 1978):

$$C_{ijkl}(f) = (1+2f)^{7/2}[C^0_{ijkl} + b_1 f] - P\Delta_{ijkl}, \tag{1.2}$$

$$b_1 = 3K_0(C'_{ijkl} + \Delta_{ijkl}) - 7C^0_{ijkl}, \tag{1.3}$$

$$\Delta_{ijkl} = -\delta_{ij}\delta_{kl} - \delta_{ik}\delta_{jl} - \delta_{il}\delta_{jk}, \tag{1.4}$$

where $f = (1/2)\left[(V_0/V)^{2/3} - 1\right]$. C^0_{ijlk} and C'_{ijlk} are the ambient-pressure elastic constants and their pressure derivatives. δ_{ij} is the Kronecker delta. The relationship between the 4-subscript and 2-subscript notations for elastic constants is described in Nye (1984).

The resulting values for the pressure derivatives of the C_{ij}s are compared with results from previous ultrasonic and Brillouin data in Table 3. Ultrasonic studies (McSkimin et al. 1965; Wang et al. 1992; Calderon et al. 2007) show wide variability in reported pressure derivative values. Considering just the elastic constants that can be determined by direct ultrasonic measurements in a single direction (C_{11}, C_{33}, C_{44}, and C_{66}), these studies show variations of 16–42 % for pressure derivatives of the longitudinal moduli and 47–269 % for pressure derivatives of the shear moduli. In contrast, the corresponding ambient-pressure moduli show only ~1 % differences among these studies. It has been shown previously that the accuracy of pressure derivatives of C_{ij}s from ultrasonic studies at modest pressure (~0.2 GPa or less) is often not reliable (Duffy et al. 1995), likely due to the limited pressure range of the measurements which cannot accurately capture the pressure dependence. Using a piston-cylinder device, Calderon et al. (2007) extended ultrasonic measurements to 1 GPa and these exhibit agreement with our pressure derivatives for some moduli (C_{12}, C_{44}), but significant disagreement with others (C_{33}) (Table 3). Thus, it appears that low-pressure (1 GPa or less) ultrasonic measurements cannot be used to obtain reliable pressure derivatives of the elastic moduli for extrapolation to higher pressure. More recently, Wang et al. (2011) used a broadband spectroscopy method in a multi-anvil press to measure two elastic moduli, C_{33} and C_{44}, of quartz up to 4.7 GPa. Our C_{33} and C_{44} values at a similar pressure (4.4 GPa) are 1.7 and 1.3 % higher, respectively, than those reported in Wang et al. (2011). Our measurements of individual C_{ij}s at high pressure are compared in Fig. 2 to a previous high-pressure Brillouin study (Gregoryanz et al. 2000) and DFT calculations (Choudhury and Chaplot 2006; Kimizuka et al. 2007). Our results are quite different from (Gregoryanz et al. 2000) especially for C_{33},

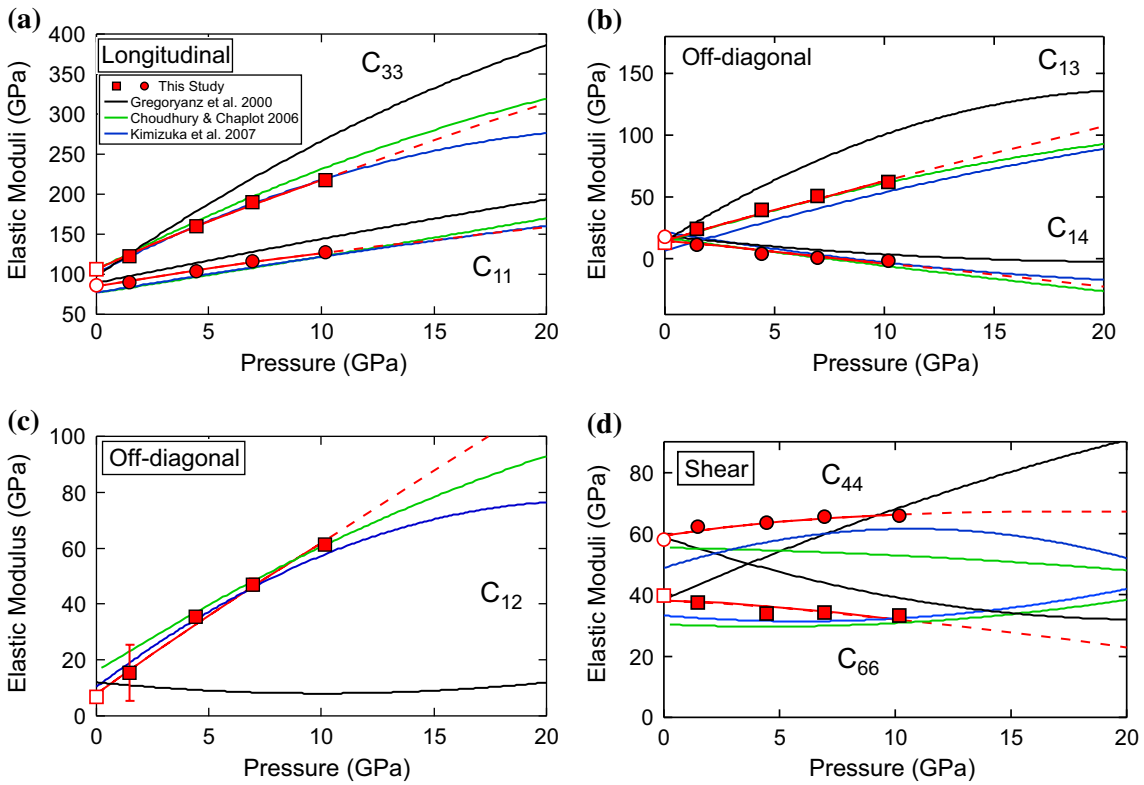

Fig. 2 **a–d** Elastic constants of α-quartz as a function of pressure. *Filled red symbols* are from this study, and *red lines* are third-order finite-strain equation fits (*solid*) extrapolated to 20 GPa (*dashed*). Data at ambient conditions (*open red symbols*) are from an average of previous studies reported in (Every and McCurdy 1992). *Black lines* show result from previous Brillouin measurements (Gregoryanz et al. 2000). *Green* (Choudhury and Chaplot 2006) and *blue* (Kimizuka et al. 2007) *lines* are from theoretical DFT calculations. In (**d**), the elastic modulus C_{66} is given by $1/2(C_{11} - C_{12})$

Table 3 Pressure derivatives of elastic moduli of α-quartz at ambient conditions

Pressure derivative	This study (Brillouin)	Gregoryanz et al. (2000) (Brillouin)	Calderon et al. (2007) (ultrasonic)	Choudhury and Chaplot (2006) (DFT)	Kimizuka et al. (2007) (DFT)	Wang et al. (1992) (ultrasonic)	McSkimin et al. (1965) (ultrasonic)
$\partial C_{11}/\partial P$	5.3 (2)	5.24	3.8	6.4	5.7	3.81	3.28
$\partial C_{33}/\partial P$	12.9 (4)	17.2	7.6	11.7	11.0	9.51	10.84
$\partial C_{12}/\partial P$	5.7 (3)	0.14	5.7	3.8	3.7	9.80	8.66
$\partial C_{13}/\partial P$	5.2 (3)	9.21	4.0	3.8	4.4	3.34	5.97
$\partial C_{14}/\partial P$	−1.7 (3)	−0.73	−1.2	−1.8	−1.7	−3.96	−1.93
$\partial C_{44}/\partial P$	1.5 (1)	−1.62	1.8	0.7	1.1	1.84	2.66
$\partial K_S/\partial P$	6.2 (2)	6.5	4.7	5.9	4.9	5.6	6.3
$\partial G/\partial P$	0.9 (1)	0.78	0.88	1.2	1.1	1.77	0.49
P_{Max} (GPa)	10	20	1	30	20	0.2	0.2

Ultrasonic = ultrasonic pulse echo overlap technique

DFT Density functional theory, P_{max} maximum pressure

The $\partial C_{ij}/\partial P$ of previous Brillouin and ultrasonic experiments are taken from those reported in Calderon et al. (2007), whereas values from DFT studies were calculated by fitting the calculated elastic constants to third-order finite-strain equations

C_{12}, and C_{13}. In particular, we obtain a value of C_{33} that is 25 % lower than the previous experiments at ~10 GPa. The results of Gregoryanz et al. (2000) may be compromised by error in crystal orientation or insufficient sampling of crystallographic directions to overcome trade-offs in elastic constants.

Our data are in better agreement with theoretical calculations (Choudhury and Chaplot 2006; Kimizuka et al. 2007), as both the experiments and calculations show similar pressure trends of the C_{ij}s. Nevertheless, there are also still differences in the magnitudes of some elastic constants between our results and theoretical studies. At 10 GPa, differences in the longitudinal elastic constants (C_{11}, C_{33}) are 2–8 %, in the shear elastic constants (C_{44}, C_{66}) are 2–14 % and in the off-diagonal constants (C_{12}, C_{13}) are 12–27 %. This is similar to the level of agreement between the theoretical values and mean experimental values (Every and McCurdy 1992) at ambient pressure which, with the exception of C_{11} and C_{33}, differ by >10 %. This is consistent with previous estimates that DFT can, in general, provide elastic constants accurate to ~15 % (Oganov et al. 2013). In summary, our results support the previous DFT results rather than earlier Brillouin results in describing the general trend of the pressure dependence of the C_{ij}s in quartz, but the approximations inherent in DFT limit the accuracy of the C_{ij} values obtained from DFT.

C_{14} is a measure of the anisotropy in the basal plane normal to the threefold symmetry axis for a trigonal crystal. A decrease in the magnitude of C_{14} with pressure indicates that the basal plane anisotropy decreases with compression in quartz, eventually reaching zero near 9 GPa (at which point the elasticity is pseudo-hexagonal), and then increasing with an opposite orientation at higher pressures. The sign of C_{14} in trigonal crystals depends on the choice of one of two options for the Cartesian coordinate system, and either a positive or negative C_{14} is physically reasonable. The axes defined in the 1988 IEEE standard on piezoelectricity (ANSI/IEEE standard 176-1988) yield a positive value for C_{14} (at ambient conditions), and we have adopted this convention. The sign of C_{14} in studies that used the opposite convention has been reversed when necessary to facilitate comparison with our work. The sign of C_{14} does not affect the value of any of the aggregate properties of quartz.

The aggregate bulk and shear moduli (Voigt-Reuss-Hill (VRH) average) were computed from the individual elastic constants (Fig. 3; Table 3). Fitting our data to finite-strain equations yields values for the pressure derivative of the adiabatic bulk modulus, K_{0S}', of 6.2(2), and the pressure derivative of the shear modulus, G_0', of 0.9(1). In contrast to the individual C_{ij}s, our aggregate bulk and shear moduli are in much better agreement with previous Brillouin results. At 10 GPa, the difference of aggregate bulk moduli between new data and previous Brillouin experiments

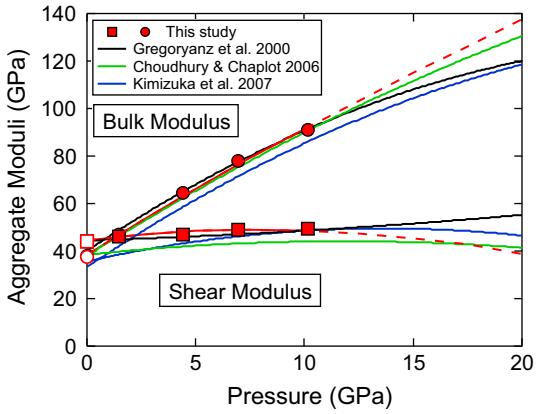

Fig. 3 Aggregate bulk and shear moduli (Voigt-Reuss-Hill) of α-quartz as a function of pressure. *Filled red symbols* are from this study with *red line* showing finite-strain fit (*solid*) extrapolated to 20 GPa (*dashed*). Ambient measurements (*open red circles*) are from (Every and McCurdy 1992). *Black lines* are from a previous high-pressure Brillouin study (Gregoryanz et al. 2000), *green* and *blue lines* are from theoretical studies (Choudhury and Chaplot 2006; Kimizuka et al. 2007)

(Gregoryanz et al. 2000) is less than 1 %. The differences in the aggregate properties are likely reduced due to averaging of the individual elastic constants. This indicates that the difference between previous experimental data and this study may be due to the trade-offs among individual elastic constants in the fitting as a result of only a single-crystal plane being measured in the earlier Brillouin study (Gregoryanz et al. 2000). Previous work has shown that such trade-offs in individual C_{ij}s tend to average out in calculating aggregate properties (Zha et al. 1998). However, it should be noted that our agreement with previous Brillouin results is restricted only to the Voigt-Reuss-Hill average, and there is considerable disagreement in the Voigt and Reuss bounds.

Our aggregate results are also in reasonable agreement with DFT studies (Choudhury and Chaplot 2006; Kimizuka et al. 2007) with differences in the Hill average of the bulk and shear moduli of ~4–5 % at 10 GPa. Our aggregate moduli extrapolated up to 20 GPa display similar trends as the earlier Brillouin and DFT studies (Fig. 3). However, the pressure derivative of the bulk modulus reported in the DFT study of Kimizuka et al. (2007) ($K_{0T}' = 4.9$) is much lower than found in this study or previous high-pressure X-ray diffraction experiments (Levien et al. 1980; Angel et al. 1997) (Table 1). The pressure derivatives of K_S and G measured here are also generally quite different from those found in the low-pressure ultrasonic studies (Table 3) further indicating that ultrasonic data should be extrapolated with caution.

Figure 4 compares the relative volume compression values of α-quartz calculated from our Brillouin measurements

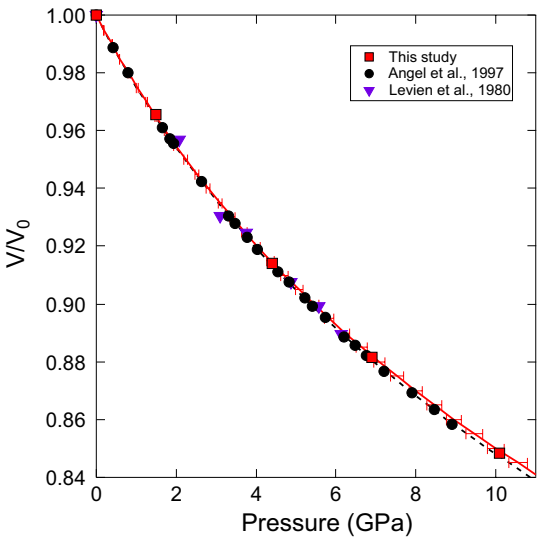

Fig. 4 Variation of relative unit cell volume with pressure. *Red squares* are from this study, and red solid line is from a fit to the third-order Birch-Murnaghan equation with $K_{0T} = 37.4(6)$ GPa, and $K'_{0T} = 6.2(2)$. Also shown are results from high-pressure X-ray diffraction experiments (Levien et al. 1980; Angel et al. 1997). *Black dashed lines* are a fit to previous diffraction data. (Angel et al. 1997) using reported values of $K_{0T} = 37.12(9)$ GPa, $K'_{0T} = 5.99(4)$. The *error bars* are calculated from propagation of the uncertainties in the Reuss bound of the bulk modulus and its pressure derivative

of this study compared with previous X-ray diffraction measurements (Levien et al. 1980; Angel et al. 1997). Here, we have used the Reuss bound of the isothermal bulk modulus to compute high-pressure densities (volumes) for comparison with X-ray diffraction data. The third-order Birch-Murnaghan fit from our Brillouin data is in agreement within uncertainty with X-ray diffraction data. The pressure derivative of the isothermal Reuss modulus obtained here ($K_{T0}' = 6.2(2)$) is consistent with values from X-ray diffraction studies ($K_{T0}' = 6.0$–6.2) (Levien et al. 1980; Angel et al. 1997).

The axial compressibilities of quartz as a function pressure can be determined from the relations:

$$\beta_a = -\mathrm{d}\ln a/\mathrm{d}P = \frac{C_{33} - C_{13}}{\Omega}, \tag{1.5}$$

and

$$\beta_c = -\mathrm{d}\ln c/\mathrm{d}P = \frac{C_{11} - C_{12} - 2C_{13}}{\Omega}, \tag{1.6}$$

where

$$\Omega = (C_{11} + C_{12})\,C_{33} - 2C_{13}^2. \tag{1.7}$$

The compressibility along a decreases by approximately a factor of 2 from 9.8×10^{-3} GPa^{-1} at 1 bar to 4.7×10^{-3} GPa^{-1} at 10.2 GPa, while the c-axis compressibility declines by nearly a factor of 4 from 7.1×10^{-3} to 1.9×10^{-3} GPa^{-1} over the same pressure range. These results are in good agreement with those from theoretical calculations (Kimizuka et al. 2007). X-ray diffraction studies show a strong increase in the *c/a* ratio with compression and yield axial compressibilities in good agreement with the experimental and theoretical elastic constants (Levien et al. 1980; Angel et al. 1997; Kimizuka et al. 2007). The underlying cause of this change in *c/a* has been attributed to the bending of Si–O–Si angles resulting in strong shortening of long O–O distances along the *a* direction (Levien et al. 1980; Hazen et al. 1989).

The elastic properties of quartz at ambient pressure are unusual in that the shear modulus ($G_0 = 44.4$ GPa) is larger than the bulk modulus ($K_{0S} = 37.8$ GPa). This results in a low value of the aggregate Poisson's ratio ($\sigma_0 = 0.08$) as in the ratio of compressional to shear velocity ($V_P/V_S = 1.5$). These have been used as diagnostics for the seismic identification of quartz-rich regions in the Earth (Christensen 1996). Upon compression, the bulk modulus of quartz increases rapidly while the shear modulus increases slowly, flattening out at higher pressures. As a result, Poisson's ratio increases rapidly to a value of $\sigma = 0.27$ while the V_P/V_S ratio increases to 1.79 at 10.2 GPa, both of these are more typical values of these quantities in silicate minerals.

When single-crystal quartz is compressed metastably at room temperature, it can undergo amorphization and/or transform to a new crystalline phase at high pressure depending on hydrostaticity and crystalline state (Machon et al. 2014). Amorphization of quartz is observed in different environments including static and dynamic laboratory experiments, meteorite impact sites, and even reportedly in ultra-high-pressure metamorphic rocks (Palmeri et al. 2009). The mechanism of formation of amorphous quartz at high pressure is not well understood. Theoretical studies have suggested that amorphization of quartz may be triggered by an elastic instability (Choudhury and Chaplot 2006). The mechanical stability of single-crystal quartz can be examined in the context of the Born stability criteria (Born and Huang 1954), which provide the necessary conditions for a crystal to be mechanically stable. For trigonal crystals, these criteria translate into the condition that the following combinations of elastic constant are positive (Carpenter and Salje 1998; Calderon et al. 2007):

$$K_1 - (C_{11} + C_{12})\,C_{33} - 2C_{13}^2 > 0, \tag{1.8}$$

$$K_2 - (C_{11} + C_{12})\,C_{44} - 2C_{14}^2 > 0, \tag{1.9}$$

There is some confusion in the literature regarding the designations for these criteria (K_1 is often referred to as 'B_2' and K_2 is referred to as 'B_3') [see (Gregoryanz et al. 2000)]. We have adopted the notation of Machon et al. (2014) here. The first criterion, K_1, expresses that the condition that sample volume cannot collapse upon compression. K_2 is associated

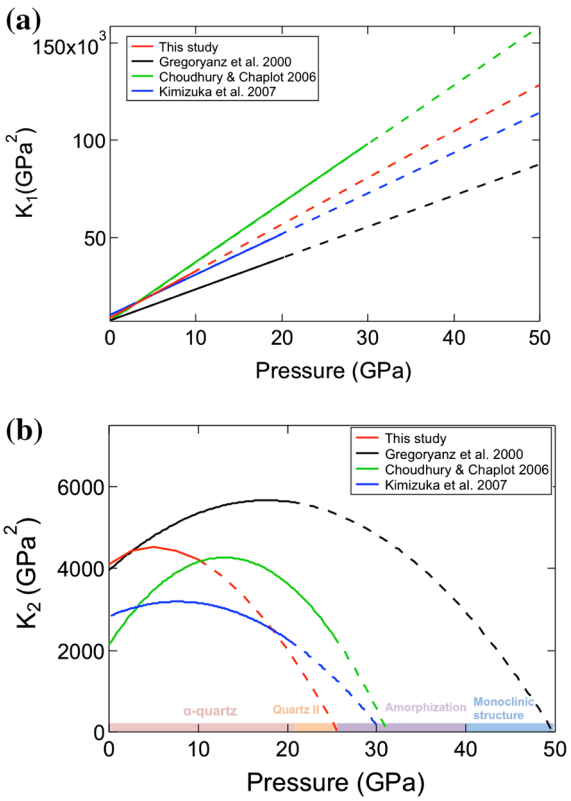

Fig. 5 **a**, **b** Born stability criteria (K_1 and K_2) of α-quartz as a function of pressure. The *red dashed line* is calculated from the extrapolation of our measured C_{ij}s The *black dashed line* is a fit from measurements and extrapolation of a previous Brillouin study (Gregoryanz et al. 2000). The *blue* and *green dashed lines* show fits from the DFT calculations (Choudhury and Chaplot 2006; Kimizuka et al. 2007). The *solid lines* are fits to the experimental and DFT data

with eigenvalues corresponding to two different acoustic modes. A negative value of K_2 under compression denotes the existence of a mechanical instability correlated with the presence of a soft acoustic shear mode in the phonon spectrum at the Γ point of the Brillouin zone (Calderon et al. 2007).

Some previous studies have suggested an instability in K_1 may be responsible for pressure-induced amorphization in quartz (Tse and Klug 1991; Calderon et al. 2007), but this is not supported by our results which show that the K_1 stability criterion is always satisfied (Fig. 5a). K_2 for quartz initially increases, reaching a maximum and then decreases. Extrapolation of this trend (using the finite-strain extrapolation of the individual elastic moduli) suggests the K_2 stability criterion will be violated at higher pressure. Figure 5b shows how the K_2 stability criterion evolves with pressure from different reported sets of high-pressure elastic constants. Our data indicate that K_2 reaches its maximum at around 10 GPa and then decreases, reaching zero at ~26 GPa, which is intermediate to the pressures of the quartz I-II transition and the observed amorphization pressure. Previous Brillouin data (Gregoryanz et al. 2000) indicate that K_2 vanishes at higher pressure (~49 GPa). DFT calculations (Choudhury and Chaplot 2006; Kimizuka et al. 2007) of the pressure at which K_2 vanishes yield values of ~30 GPa. Overall, the DFT studies and our high-pressure measurements provide a broadly consistent picture of the behavior of the stability criterion K_2 which is in general accord with the observed amorphization pressure.

Conclusion

Measurement of the single-crystal elastic moduli of α-quartz was undertaken to resolve discrepancies among previous experimental and theoretical studies. Our new results for the individual C_{ij}s agree qualitatively with DFT calculations but not with previous high-pressure Brillouin data. However, the Voigt-Reuss-Hill average of the aggregate bulk and shear moduli are in better agreement with both previous experimental and theoretical studies than the individual elastic moduli. Pressure derivatives obtained from ultrasonic elasticity studies at less than or equal to 1 GPa are not consistent with each other but results from more recent study by Calderon et al. (2007) are close to our new measurements for four of the six individual moduli. Densities inferred from our Brillouin data at high pressure match previous X-ray diffraction data within uncertainties. The high-pressure elastic constants of quartz provide insights into the connection between Born stability criteria, and elastic instabilities in α-quartz related to pressure-induced amorphization.

Acknowledgments This research was supported by the NSF and the Carnegie-DOE Alliance Center.

References

Ackerman RJ, Sorrell C (1974) Thermal-expansion and high-low transformation in quartz.1. High-temperature X-ray studies. J Appl Crystallogr 7:461–467. doi:10.1107/S0021889874010211

Angel RJ, Allan DR, Miletich R, Finger LW (1997) The use of quartz as an internal pressure standard in high-pressure crystallography. J Appl Crystallogr 30:461–466. doi:10.1107/S0021889897000861

Angel RJ, Bujak M, Zhao J et al (2007) Effective hydrostatic limits of pressure media for high-pressure crystallographic studies. J Appl Crystallogr 40:26–32. doi:10.1107/S0021889806045523

ANSI/IEEE standard 176-1988 (1988) IEEE Standard on Piezoelectricity. Institute of Electrical and Electronic Engineers, New York

Ballato A (2008) Basic material quartz and related innovations. Piezoelectricity. Springer, Berlin, pp 9–35

Binggeli N, Chelikowsky J (1992) Elastic instability in alpha-quartz under pressure. Phys Rev Lett 69:2220–2223. doi:10.1103/PhysRevLett.69.2220

Binggeli N, Keskar N, Chelikowsky J (1994) Pressure-induced amorphization, elastic instability, and soft modes in alpha-quartz. Phys Rev B 49:3075–3081. doi:10.1103/PhysRevB.49.3075

Birch F (1978) Finite strain isotherm and velocities for single-crystal and polycrystalline NaCl at high-pressures and 300-degree-K. J Geophys Res 83:1257–1268. doi:10.1029/JB083iB03p01257

Born M, Huang K (1954) Dynamical theory of crystal lattices. Oxford University Press, London

Calderon E, Gauthier M, Decremps F et al (2007) Complete determination of the elastic moduli of α-quartz under hydrostatic pressure up to 1 GPa: an ultrasonic study. J Phys: Condens Matter 19:436228. doi:10.1088/0953-8984/19/43/436228

Carpenter MA, Salje EKH (1998) Elastic anomalies in minerals due to structural phase transitions. Eur J Miner 10:693–812

Choudhury N, Chaplot SL (2006) Ab initio studies of phonon softening and high-pressure phase transitions of α-quartz SiO_2. Phys Rev B 73:094304. doi:10.1103/PhysRevB.73.094304

Christensen NI (1996) Poisson's ratio and crustal seismology. J Geophys Res 101:3139. doi:10.1029/95JB03446

Duffy TS, Zha C, Downs RT et al (1995) Elasticity of forsterite to 16 GPa and the composition of the upper mantle. Nature 378:170–173. doi:10.1038/378170a0

Every AG (1980) General closed-form expressions for acoustic-waves in elastically anisotropic solids. Phys Rev B 22:1746–1760. doi:10.1103/PhysRevB.22.1746

Every AG, McCurdy AK (1992) The elastic constants of crystals. In: Nelson DF (ed) Landolt-Börnstein tables III29. Springer, Berlin/Heidelberg, pp 1–634

Glinnemann J, King HE, Schulz H et al (1992) Crystal structures of the low-temperature quartz-type phases of SiO_2 and GeO_2 at elevated pressure. Z Für Krist 198:177–212. doi:10.1524/zkri.1992.198.3-4.177

Gregoryanz E, Hemley RJ, Mao H-k, Gillet P (2000) High-pressure elasticity of α-quartz: instability and ferroelastic transition. Phys Rev Lett 84:3117–3120. doi:10.1103/PhysRevLett.84.3117

Haines J, Léger JM, Gorelli F, Hanfland M (2001) Crystalline post-quartz phase in silica at high pressure. Phys Rev Lett 87:155503. doi:10.1103/PhysRevLett.87.155503

Hazen RM, Finger LW, Hemley RJ, Mao HK (1989) High-pressure crystal chemistry and amorphization of α-quartz. Solid State Commun 72:507–511. doi:10.1016/0038-1098(89)90607-8

Heaney PJ, Prewitt CT, Gibbs GV (1994) Silica: physical behavior, geochemistry and materials applications. Rev Mineralogy, 29 Mineralogical Society of America, Washington, DC

Hemingway BS (1987) Quartz-heat-capacities from 340-K to 1000-K and revised values for the thermodynamic properties. Am Miner 72:273–279

Hemley RJ (1987) Pressure dependence of Raman spectra of SiO_2 polymorphs: α-quartz, coesite, and stishovite. In: Manghnani H, Syono M (eds) High-pressure research in mineral physics. American Geophysical Union, pp 347–359

Hemley RJ, Jephcoat AP, Mao H-k et al (1988) Pressure-induced amorphization of crystalline silica. Nature 334:52–54. doi:10.1038/334052a0

Hemley RJ, Prewitt CT, Kingma KJ (1994) High-pressure behavior of silica. In: PJ Heaney, CT Prewitt, GV Gibbs (eds) Silica: physical behavior, geochemistry and materials applications. Rev Mineralogy, 29 Rev. Mineral. Geochem. pp 41–81

Heyliger P, Ledbetter H, Kim S (2003) Elastic constants of natural quartz. J Acoust Soc Am 114:644. doi:10.1121/1.1593063

Hill R (1963) Elastic properties of reinforced solids: some theoretical principles. J Mech Phys Solids 11:357–372. doi:10.1016/0022-5096(63)90036-X

Holm B, Ahuja R (1999) Ab initio calculation of elastic constants of SiO_2 stishovite and α-quartz. J Chem Phys 111:2071–2074. doi:10.1063/1.479475

Kimizuka H, Ogata S, Li J, Shibutani Y (2007) Complete set of elastic constants of α-quartz at high pressure: a first-principles study. Phys Rev B 75:054109. doi:10.1103/PhysRevB.75.054109

Kingma K, Hemley R, Mao H-k, Veblen D (1993a) New high-pressure transformation in alpha-quartz. Phys Rev Lett 70:3927–3930. doi:10.1103/PhysRevLett.70.3927

Kingma K, Meade C, Hemley R et al (1993b) Microstructural observations of alpha-quartz amorphization. Science 259:666–669

Lakshtanov DL, Sinogeikin SV, Bass JD (2006) High-temperature phase transitions and elasticity of silica polymorphs. Phys Chem Miner 34:11–22. doi:10.1007/s00269-006-0113-y

Levien L, Prewitt CT, Weidner DJ (1980) Structure and elastic properties of quartz at pressure. Am Mineral 65:920–930

Machon D, Meersman F, Wilding MC et al (2014) Pressure-induced amorphization and polyamorphism: inorganic and biochemical systems. Prog Mater Sci 61:216–282. doi:10.1016/j.pmatsci.2013.12.002

Mao HK, Xu J, Bell PM (1986) Calibration of the ruby pressure gauge to 800-Kbar under quasi-hydrostatic conditions. J Geophys Res 91:4673–4676. doi:10.1029/JB091iB05p04673

McSkimin HJ, Andreatch P Jr, Thurston RN (1965) Elastic moduli of quartz versus hydrostatic pressure at 25 and −195.8 C. J Appl Phys 36:1624–1632. doi:10.1063/1.1703099

Mirwald PW, Massonne H-J (1980) The low-high quartz and quartz-coesite transition to 40 kbar between 600 and 1600 C and some reconnaissance data on the effect of NaAlO2 component on the low quartz-coesite transition. J Geophys Res Solid Earth 85:6983–6990. doi:10.1029/JB085iB12p06983

Nye JF (1984) Physical properties of crystals: their representation by tensors and matrices. Clarendon Press, Oxford University Press, Oxford

Oganov AR, Hemley RJ, Hazen RM, Jones AP (2013) Structure, bonding, and mineralogy of carbon at extreme conditions. In: Hazen RM, Jones AP, Baross JA (eds) Rev. Mineral, Geochem, pp 47–77

Ogi H, Ohmori T, Nakamura N, Hirao M (2006) Elastic, anelastic, and piezoelectric coefficients of α-quartz determined by resonance ultrasound spectroscopy. J Appl Phys 100:053511. doi:10.1063/1.2335684

Ohno I (1990) Rectangular parallelepiped resonance method for piezoelectric-crystals and elastic-constants of alpha-quartz. Phys Chem Miner 17:371–378

Ohno I (1995) Temperature-variation of elastic properties of alpha-quartz up to the alpha–beta transition. J Phys Earth 43:157–169

Ohno I, Harada K, Yoshitomi C (2006) Temperature variation of elastic constants of quartz across the α–β transition. Phys Chem Miner 33:1–9. doi:10.1007/s00269-005-0008-3

Palmeri R, Frezzotti ML, Godard G, Davies RJ (2009) Pressure-induced incipient amorphization of α-quartz and transition to coesite in an eclogite from Antarctica: a first record and some consequences. J Metamorph Geol 27:685–705. doi:10.1111/j.1525-1314.2009.00843.x

Speziale S, Duffy TS (2002) Single-crystal elastic constants of fluorite (CaF_2) to 9.3 GPa. Phys Chem Miner 29:465–472. doi:10.1007/s00269-002-0250-x

Tarumi R, Nakamura K, Ogi H, Hirao M (2007) Complete set of elastic and piezoelectric coefficients of α-quartz at low temperatures. J Appl Phys 102:113508. doi:10.1063/1.2816252

Tse J, Klug D (1991) Mechanical instability of alpha-quartz—a molecular-dynamics study. Phys Rev Lett 67:3559–3562. doi:10.1103/PhysRevLett.67.3559

Wang Q, Saunders GA, Lambson EF et al (1992) Temperature dependence of the acoustic-mode vibrational anharmonicity of quartz from 243 to 393 K. Phys Rev B 45:10242–10254. doi:10.1103/PhysRevB.45.10242

Wang Z, Liu Y, Song W et al (2011) A broadband spectroscopy method for ultrasonic wave velocity measurement under high pressure. Rev Sci Instrum 82:014501. doi:10.1063/1.3518953

Whitfield CH, Brody EM, Bassett WA (1976) Elastic moduli of NaCl by Brillouin scattering at high pressure in a diamond anvil cell. Rev Sci Instrum 47:942–947. doi:10.1063/1.1134778

Williams Q, Hemley R, Kruger M, Jeanloz R (1993) High-pressure infrared-spectra of alpha-quartz, coesite, stishovite and silica Glass. J Geophys Res-Solid Earth 98:22157–22170. doi:10.1029/93JB02171

Zha CS, Duffy TS, Downs RT et al (1998) Brillouin scattering and X-ray diffraction of San Carlos olivine: direct pressure determination to 32 GPa. Earth Planet Sci Lett 159:25–33. doi:10.1016/S0012-821X(98)00063-6

Zouboulis IS, Jiang F, Wang J, Duffy TS (2014) Single-crystal elastic constants of magnesium difluoride (MgF_2) to 7.4 GPa. J Phys Chem Solids 75:136–141. doi:10.1016/j.jpcs.2013.09.014

Original publication:

Wang, J., Z. Mao, F. Jiang, and T. S. Duffy, Elasticity of single-crystal quartz to 10 GPa, *Physics and Chemistry of Minerals*, 42, 203-212, 2015.

Correction

In this publication, the values of the Voigt-Reuss-Hill averages for the adiabatic bulk moduli (K_S) and the shear moduli (G) were listed incorrectly. The corrected values are listed below.

Table 2. Elastic constants of α-quartz.

P (GPa)	ρ (g/cm^3)	C_{11} (GPa)	C_{33} (GPa)	C_{12} (GPa)	C_{13} (GPa)	C_{14} (GPa)	C_{44} (GPa)	K_S (GPa)	G (GPa)	RMS (km/s)
10^{-4}	2.648	86.6 (3)	106.4 (12)	6.74 (9)	12.4 (16)	17.8 (3)	58.0 (7)	37.8	44.4	
1.5	2.742	90.3 (8)	122.3 (15)	15.4 (100)	23.7 (21)	10.7 (10)	62.4 (10)	46.9	46.1	0.087
4.4	2.897	103.4 (3)	160.1 (10)	35.6 (6)	38.9 (10)	3.8 (7)	63.6 (4)	64.6	47.0	0.040
6.9	3.004	115.7 (20)	190.6 (19)	47.1 (20)	50.6 (14)	0.3 (1)	65.4 (5)	77.8	48.9	0.058
10.2	3.120	127.5 (5)	217.0 (10)	61.3 (7)	62.0 (12)	-1.9 (8)	65.9 (3)	91.2	49.2	0.054

For C_{ij}s, numbers in parentheses represent one standard deviation uncertainties in the last digit.
Ambient values are an average of 12 previous studies compiled in Every and McCurdy (1992).
K_S and G refer to Voigt-Reuss-Hill averages of the individual elastic moduli.
ANSI/IEEE Standard 176-1988 is used to assign the sign of C_{14}.
RMS: root mean square deviation between measured and best-fit velocities.